

Second law analysis in MHD flow and heat transfer of a rotating Casson fluid over a stretching surface

Shalini Jain* & Rakesh Choudhary

Department of Mathematics & Statistics, Manipal University Jaipur, Jaipur 303 007, India

Received 15 June 2017; accepted 3 November 2017

Second law analysis in three-dimensional MHD boundary layer flow and heat transfer of a rotating Casson fluid over a stretching surface has been investigated. Such flow problems have relevance in extraction and manufacturing of rubber and polymer sheets. Solution of these problems is of great interest as they serve a practical purpose. Partial differential equations governing flow and heat transfer have been transformed into non-linear ordinary differential equations by using suitable similarity transformations. These non-linear differential equations have been solved numerically by using shooting techniques with fourth order Runge-Kutta method. Effects of Casson fluid parameter β , rotation parameter λ , Prandtl number Pr and magnetic field parameter M on velocity profile, temperature profile and skin friction number have been analyzed and depicted through graphs and tables. Entropy generation number and Bejan number have also been obtained and discussed.

Keywords: Rotating Casson fluid, Heat transfer, Stretching surface, Entropy generation, Runge-Kutta method

1 Introduction

Flow induced by stretching surfaces has often encountered in several engineering and industrial processes and therefore its study has many promising applications for example in extraction and manufacturing of rubber and polymer sheets, wire and fiber cutting process, design of various equipment used in chemical and food stuff processing. Mechanical properties of such products depend on rate of heat transfer at the stretching sheet. Initially Crane¹ examined boundary layer flow expulsion by the continuous stretching of a surface in a fixed point. Sakiadis² initiated the effects of boundary layer flow past a moving surface. Wang³ extended Crane's problem and examined three-dimensional flow due to a stretching flat surface. Verma and Chauhan⁴ studied flow between a torsionally oscillating impermeable disc and a stationary naturally permeable disc. Many researchers such as Jain⁵, Fang *et al.*⁶, Najjar *et al.*⁷, Mahanta and Shaw⁸, Jain and Choudhary⁹, Raju *et al.*¹⁰ and Jain and Bohra¹¹ investigated heat transfer phenomena on flow over a stretching sheet. Rotating fluid flows in boundary layer flows have several applications in areas like astrophysical process, biomechanics, cosmic fluid dynamics, industrial processes, in the design of turbines and rotating heat exchangers etc.

Rotating fluid flows can also be observed at the migration of underwater and movement of oil, petrol and gas through reservoirs. Wang¹² obtained exact results for a stretching surface in a rotating fluid. Takhar *et al.*¹³ studied flow over a stretching surface in a rotating fluid with a magnetic field. Zaimi *et al.*¹⁴ analyzed heat transfer effects of rotating viscoelastic fluid in stretching surface. Recently, Mustafa¹⁵ and Hayat *et al.*¹⁶ also studied the heat transfer effects of nanofluids in a rotating systems with MHD.

Second law analysis is basic for many of engineering motives for formulating and solving convection problems. For example, in the development of know how for the heat exchanger industry. We strive for improved thermal contact and reduced pump power loss in order to improve thermodynamic efficiency of a heat exchanger. A good heat exchanger means minimum generation of entropy. Bejan¹⁷ played a very important role to investigate the entropy generation effects. The ideas of Bejan became a milestone for every researcher. Makinde and Osalusi¹⁸ studied entropy analysis of laminar flow in a filled channel embedded in a saturated porous medium. Butt and Ali¹⁹ examined investigation of entropy generation effects in MHD three-dimensional flow and heat transfer of viscous fluid over a stretching surface. Recently, Freidoonimehr *et al.*²⁰ and Qing *et al.*²¹ investigated entropy generation analysis of a MHD Casson fluid

*Corresponding author (E-mail:shalini.jain@jaipur.manipal.edu)

over a rotating disk and porous stretching/shrinking sheet, respectively.

Several fluids used in industrial and engineering process such as geological materials and poly liquid foams, exhibit flow properties that are difficult to explain by the Newtonian model. One such model is the non-Newtonian Casson fluid model which symbolizes a shear thinning fluid which is assumed to have infinite viscosity at zero rate of shear. This fluid behaves like solid elastic and has yield shear stress in the consecutive equation for a Casson fluid²². Analysis of the Casson and Carreau-Yasuda non-Newtonian blood models in steady and oscillatory flow was discussed by Boyd *et al.*²³ who used the lattice Boltzmann method for this purpose. Examples of a Casson fluid are jelly, honey, soup and human blood. Flow and heat transfer phenomena of a Casson fluid having different physical and mathematical aspects was analyzed by several researchers such as Bhargava *et al.*²⁴, Attia and Ahmed²⁵ and Mukhopadhyay²⁶. Nadeem *et al.*²⁷ discussed heat transfer and MHD boundary layer flow effects of a Casson fluid past an exponentially shrinking sheet. Bhattacharyya *et al.*²⁸ studied an analytical solution for MHD boundary layer flow of a Casson fluid over a stretching/shrinking sheet with wall mass transfer. Mukhopadhyay *et al.*²⁹ discussed Casson fluid flow and heat transfer past a symmetric wedge. MHD three-dimensional Casson fluid past a porous linearly stretching sheet was analyzed by Nadeem *et al.*³⁰. Pramanik³¹ investigated heat transfer effects of Casson fluid flow over an exponentially porous stretching surface with thermal radiation. Tufail *et al.*³² studied heat source/sink effects on non-Newtonian magnetohydrodynamic fluid flow over a permeable stretching surface. Sumalatha and Bandari³³ analyzed heat transfer effects of Casson fluid flow over a nonlinear stretching sheet. Several authors have studied the Casson fluid model under different geometries such as Butt *et al.*³⁴, Jain and Bohra³⁵, Ali *et al.*³⁶ and Raju *et al.*³⁷.

The forgoing discussion that deal with a rotating Casson fluid with stretching surface are restricted to the first law of thermodynamics and, to the best of our knowledge, none of them investigated the second law of thermodynamics. Recently Butt *et al.*³⁴ studied of flow and heat transfer on a stretching surface in a rotating Casson fluid. In this paper we extend the work of Butt *et al.*³⁴ and aim to investigate entropy generation of flow and heat transfer over a stretching

surface under transverse magnetic field, in a rotating Casson fluid.

Governing equations are solved numerically and results obtained for pertinent parameters are discussed and presented through graphs and tables.

2 Flow Analysis

Consider steady, three-dimensional, laminar incompressible MHD boundary layer flow of a rotating Casson fluid over a stretching surface. Assume that the surface is stretched in the *x*-direction. The velocity components *u*, *v* and *w* are in the direction of the *x*, *y* and *z* axes, respectively, with an angular velocity ω in the *z* direction (Fig. 1). B_0 is a magnetic field which is applied normal to the surface. The Coriolis force is the reason for flow in three dimensional MHD boundary layer flow. The fluid rotates with angular velocity ω about the *z* axis. Let T_w be the constant temperature of the stretching surface and T_∞ be the temperature of the fluid far away.

Rheological model that describes Casson fluid is:

$$\tau_{ij} = \begin{cases} 2(\mu_B + p_y / \sqrt{2\pi})e_{ij}, \pi > \pi_c \\ 2(\mu_B + p_y / \sqrt{2\pi_c})e_{ij}, \pi < \pi_c \end{cases} \dots (1)$$

where τ_{ij} is the component of the stress tensor, p_y is the yield stress of the fluid, π is the product of the component of the deformation rate with itself, π_c is a critical value of this product based on the non-Newtonian model and μ_B is the plastic dynamic velocity of the non-Newtonian fluid.

The governing equations following Butt and Ali¹⁹ are given as:

Equation of continuity:

$$\frac{\partial u}{\partial x} + \frac{\partial v}{\partial y} + \frac{\partial w}{\partial z} = 0 \dots (2)$$

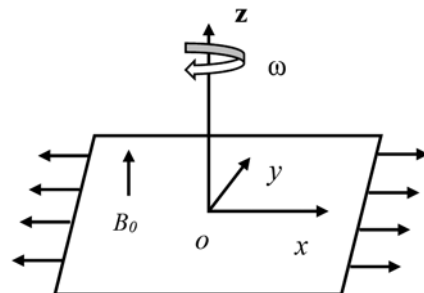


Fig. 1 — Schematic diagram of the problem.

Equation of momentum:

$$u \frac{\partial u}{\partial x} + v \frac{\partial u}{\partial y} + w \frac{\partial u}{\partial z} - 2\omega v = -\frac{1}{\rho} \frac{\partial p}{\partial x} + \nu \left(1 + \frac{1}{\beta}\right) \nabla^2 u - \frac{\sigma B_0^2 u}{\rho} \quad \dots (3)$$

$$u \frac{\partial v}{\partial x} + v \frac{\partial v}{\partial y} + w \frac{\partial v}{\partial z} + 2\omega u = -\frac{1}{\rho} \frac{\partial p}{\partial y} + \nu \left(1 + \frac{1}{\beta}\right) \nabla^2 v - \frac{\sigma B_0^2 v}{\rho} \quad \dots (4)$$

$$u \frac{\partial w}{\partial x} + v \frac{\partial w}{\partial y} + w \frac{\partial w}{\partial z} = -\frac{1}{\rho} \frac{\partial p}{\partial z} + \nu \left(1 + \frac{1}{\beta}\right) \nabla^2 w - \frac{\sigma B_0^2 w}{\rho} \quad \dots (5)$$

Equation of energy:

$$u \frac{\partial T}{\partial x} + v \frac{\partial T}{\partial y} + w \frac{\partial T}{\partial z} = \frac{k}{\rho C_p} \nabla^2 T + \frac{\nu}{C_p} \left(1 + \frac{1}{\beta}\right) \left[\left(\frac{\partial u}{\partial z}\right)^2 + \left(\frac{\partial v}{\partial z}\right)^2 \right] \quad \dots (6)$$

Subject to boundary conditions:

$$u = u_w(x) = ax, v = 0, w = 0, T = T_w \quad \text{at} \quad z = 0$$

and $u \rightarrow 0, v \rightarrow 0, T \rightarrow T_\infty$ at $z \rightarrow \infty$... (7)

where $a > 0$ is constant, $\beta = \frac{\mu_B \sqrt{2\pi_c}}{p_y}$ is the Casson fluid parameter, ν is the kinematic viscosity, k is thermal conductivity, C_p is the specific heat of the fluid at a constant pressure, ρ is the density and T is the temperature of the fluid.

We introduce the similarity transformation so that the continuity equation is identically satisfied.

We define:

$$u = ax f'(\eta), \quad v = ax g(\eta) \quad \text{and} \quad w = -\sqrt{av} f(\eta),$$

$$\eta = \sqrt{\frac{a}{\nu}} z, \quad \theta = \frac{T - T_\infty}{T_w - T_\infty} \quad \dots (8)$$

Substituting Eq. (8) in Eqs (2-6), Eq. (2) is satisfied and Eqs (3, 4, 6) become:

$$\left(1 + \frac{1}{\beta}\right) f'''' + ff'' + 2\lambda g - Mf' - f'^2 = 0 \quad \dots (9)$$

$$\left(1 + \frac{1}{\beta}\right) g'' - f'g + fg' - 2\lambda f' - Mg = 0 \quad \dots (10)$$

$$\theta'' + Pr f\theta' + \left(1 + \frac{1}{\beta}\right) Pr Ec (f'^2 + g'^2) = 0 \quad \dots (11)$$

where $M = \frac{\sigma B_0^2}{\rho a}$ is the magnetic field parameter,

$\lambda = \frac{\omega}{a}$ is the ratio of rate of rotation to stretching rate,

$Pr = \frac{\mu C_p}{k}$ is the Prandtl number and $Ec = \frac{u_w^2}{C_p (T_w - T_\infty)}$

is the local Eckert number. Here η is only function of z and it does not depend on x . Hence the Eckert number (Ec) does not depend only on the physical property but it increases with the square of the velocity.

The corresponding boundary conditions reduced to:

$$f'(0) = 1, f(0) = 0, g(0) = 0, \theta(0) = 1, \text{ and}$$

$$f'(\infty) = 0, g(\infty) = 0, \theta(\infty) = 0 \quad \dots (12)$$

The skin friction coefficients along with x and y directions are as follows:

$$C_{fx} = \frac{\tau_{wx}}{\rho u_w^2}, \quad C_{fy} = \frac{\tau_{wy}}{\rho u_w^2}, \quad \dots (13)$$

where τ_{wx} and τ_{wy} are the surface shear stress along the x and y directions, respectively, and are defined as:

$$\tau_{wx} = \left(\mu_B + \frac{p_y}{\sqrt{2\pi}} \right) \left(\frac{\partial u}{\partial z} \right)_{z=0},$$

$$\tau_{wy} = \left(\mu_B + \frac{p_y}{\sqrt{2\pi}} \right) \left(\frac{\partial v}{\partial z} \right)_{z=0}. \quad \dots (14)$$

By using Eqs (8) and (14), we get:

$$\sqrt{Re_x} C_{fx} = \left(1 + \frac{1}{\beta}\right) f''(0), \quad \sqrt{Re_x} C_{fy} = \left(1 + \frac{1}{\beta}\right) g'(0) \quad \dots (15)$$

The local Nusselt number Nu_x is defined as follows:

$$Nu_x = \frac{xq_w}{k(T_w - T_\infty)} \quad \dots (16)$$

where $q_w = -k \left(\frac{\partial T}{\partial z} \right)_{z=0}$ is the heat flux. Substituting the value of q_w in Eq. (16), then the non-dimensional of Nusselt number is as follows:

$$\frac{Nu_x}{\sqrt{Re_x}} = -\theta'(0) \quad \dots (17)$$

3 Numerical Solution

The boundary value problems given in Eqs (9-11) are solved by the forth order Runge-Kutta Shooting method. The important steps for this method are as follows:

Convert the boundary value problem into the initial value problem.

Reduce the system of Eqs (9-11) into a first order system.

We assume that c_1, c_2 and c_3 are the initial guesses for $f''(0), g'(0)$ and $\theta'(0)$, respectively. For this we consider a finite domain $0 \leq \eta \leq \eta_\infty$ instead of semi-infinite integration domain $0 \leq \eta \leq \infty$. where η_∞ has been chosen sufficiently large so that solution obtained closely approximates the boundary condition. In this study we have considered $\eta_\infty = 10$. The boundary value problem is converted into a system of initial value problems, as given below:

$$\begin{aligned} f' &= z, z' = p, p' = \frac{1}{1 + \frac{1}{\beta}} (-fp - 2\lambda g + Mz + z^2), \\ g' &= v, v' = \frac{1}{1 + \frac{1}{\beta}} (zg - fv + 2\lambda z + Mg) \\ \theta' &= q, q' = -Pr fq - \left(1 + \frac{1}{\beta} \right) Pr Ec (p^2 + v^2) \end{aligned} \quad \dots (18)$$

Subject to boundary conditions:

$$\begin{aligned} f(0) &= 0, z(0) = 1, g(0) = 0, \\ p(0) &= c_1, v(0) = c_2, \theta(0) = 1, q(0) = c_3 \quad \dots (19) \end{aligned}$$

4 Entropy Generation

Bejan¹⁷ described the local entropy generation rate per unit volume S^G for a viscous fluid in the presence of magnetic field. Entropy generation equation for a Casson fluid is as follows:

$$\begin{aligned} S^G &= \frac{k}{T_\infty^2} \left(\frac{\partial T}{\partial z} \right)^2 + \frac{\mu}{T_\infty} \left(1 + \frac{1}{\beta} \right) \\ &\left[\left(\frac{\partial u}{\partial z} \right)^2 + \left(\frac{\partial v}{\partial z} \right)^2 \right] + \frac{\sigma B_0^2}{T_\infty} (u^2 + v^2) \end{aligned} \quad \dots (20)$$

The first term in Eq. (20) is due to heat transfer. The second term is due to fluid friction irreversibility and the third terms denote the magnetic field.

To obtain anon-dimensional form of Eq. (20), we define the characteristic entropy generation rate:

$$S_0^G = \frac{k \Delta T^2}{T_\infty^2 x^2} \quad \dots (21)$$

The non-dimensional entropy generation number is as follows:

$$\begin{aligned} N_s &= \frac{S^G}{S_0^G} = Re_x \theta'^2 + \left(1 + \frac{1}{\beta} \right) \\ &\frac{1}{\Omega} Br Re_x (f'^2 + g'^2) + \frac{1}{\Omega} Br Re_x M (f'^2 + g'^2) \end{aligned} \quad \dots (22)$$

where $Re_x = \frac{u_w x}{\nu}$ is the local Reynolds number,

$$Br = \frac{\mu u_w^2}{k(T_w - T_\infty)}$$

is the Brinkmann number, $\Omega = \frac{\Delta T}{T_\infty}$

is the dimensionless temperature difference.

Eq. (22) can be rewritten in the form:

$$N_s = N_H + N_f + N_m = N_H + N_F \quad \dots (23)$$

where N_H is entropy generation due to heat transfer, N_f is entropy generation due to fluid friction and N_m shows entropy effects due to magnetic field.

The Bejan number is described as follows:

$$Be = \frac{N_H}{N_H + N_F} \quad \dots (24)$$

From Eq. (24) it is clear that the range for the Bejan number is between 0 and 1. Also when $Be = \frac{1}{2}$ the entropy due to heat transfer fluid friction and magnetic field entropy are equal.

5 Results and Discussion

Equations (9-11) subject to boundary condition (Eq. (12)) have been solved numerically using Runge-Kutta fourth order with shooting method.

Tables (1-3) show a comparison between present results and existing results of Wang¹², Najar⁷ and Butt *et al.*³⁴. It is clearly seen that our results are very well in agreement with existing results. It is observed that our results are well in agreement with Butt *et al.*³⁴ for particular conditions of our problem. Figures 2 and 3 show a comparison between our work and Butt *et al.*³⁴ for velocity and temperature profiles.

Figures 4 and 5 show velocity profiles $f'(\eta)$ and $g(\eta)$ in the x and y directions for magnetic parameter M . An increase in magnetic field reduces the velocity component in both the x and y direction of stretching surface, due to an increase in Lorentz force, which offers greater resistance to the flow, and hence flow decelerates. However, in Fig. 6, with an increase in magnetic field M , temperature increases. The Casson parameter also reduces velocity boundary layer. This is due to the introduction of tensile stress. Elasticity creates resistance in the fluid flow, and as a result velocity decreases. For higher values of Casson fluid parameter β , there is a decrease in thickness of the momentum boundary layer. However, with increase in β , the thermal boundary layer thickness increases.

Figures 7-9 indicate the effect of the Casson fluid parameter β on velocity profile and temperature profile.

The velocity profiles $f'(\eta)$ and $g(\eta)$ decrease with the increasing values of the Casson fluid parameter β . For higher values of β the boundary layer thickness decreases. An increase in the Casson fluid parameter β the temperature profile $\theta(\eta)$ increases. In Fig. 9 at a particular set of parameters, when magnetic field parameter $M=0$ and Prandtl Number $Pr = 20$, the results obtained are exactly the same as those mentioned by Butt *et al.*³⁴

Figures 10 and 11 depict the effect of rotation parameter λ on velocity profiles $f'(\eta)$ and $g(\eta)$. With an

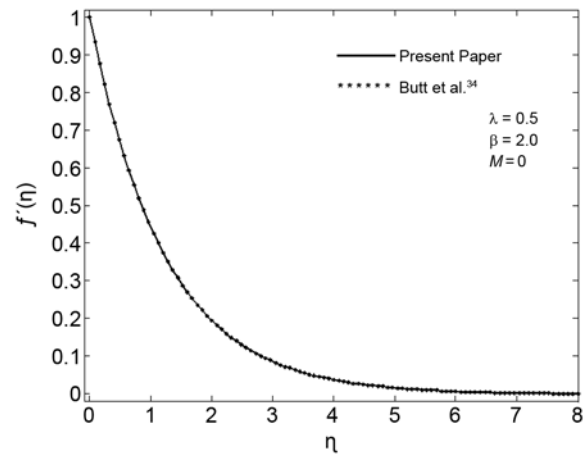


Fig. 2 — Comparison of velocity profile.

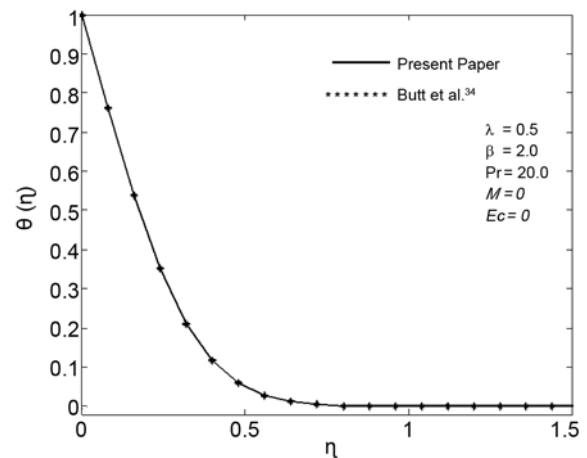


Fig. 3 — Comparison of temperature profile.

Table 1 — Comparison of the values of $f''(0)$ when $M=0$ and $\beta \rightarrow \infty$.

λ	Wang ¹² $f''(0)$	Najar <i>et al.</i> ⁷ $f''(0)$	Butt <i>et al.</i> ³⁴ $f''(0)$	Present Study $f''(0)$
0.0	-1.0000	-1.0000	-1.0000	-1.000000
0.5	-1.1384	-1.1384	-1.1384	-1.138389
1.0	-1.3250	-1.3250	-1.3250	-1.325058
2.0	-1.6523	-1.6523	-1.6523	-1.652373

Table 2 — Comparison of the values of $g'(0)$ when $M=0$ and $\beta \rightarrow \infty$.

λ	Wang ¹² $g'(0)$	Najar <i>et al.</i> ⁷ $g'(0)$	Butt <i>et al.</i> ³⁴ $g'(0)$	Present Study $g'(0)$
0.0	0.0000	0.0000	0.0000	0.000000
0.5	-0.5128	-0.5128	-0.5128	-0.512752
1.0	-0.8371	-0.8371	-0.8371	-0.837072
2.0	-1.2873	-1.2873	-1.2873	-1.287236

Table 3 — Comparison of the values of $\theta'(0)$ when $M=0, Ec=0$ and $\beta \rightarrow \infty$.

λ	Pr = 0.7			Pr = 2.0			Pr = 7.0		
	Wang ¹²	Butt <i>et al.</i> ³⁴	Present study	Wang ¹²	Butt <i>et al.</i> ³⁴	Present study	Wang ¹²	Butt <i>et al.</i> ³⁴	Present study
0.0	-0.455	-0.454	-0.4539	-0.911	-0.911	-0.9113	-1.894	-1.895	-1.8954
0.5	-0.390	-0.389	-0.3893	-0.853	-0.852	-0.8524	-1.850	-1.851	-1.8511
1.0	-0.321	-0.321	-0.3221	-0.770	-0.770	-0.7703	-1.788	-1.788	-1.7876
2.0	-0.242	-0.242	-0.2481	-0.638	-0.638	-0.6377	-1.664	-1.664	-1.6643

increase in the value of λ the velocity profile $f'(\eta)$ decreases and the boundary layer thickness decreases. Similarly for velocity profile $g(\eta)$ when we increase the rotation parameter λ the velocity profile $g(\eta)$

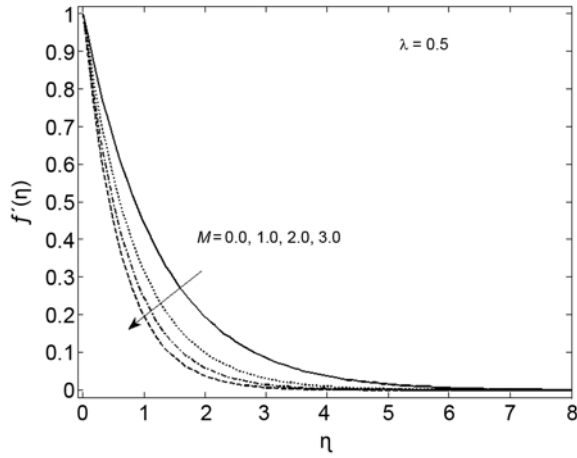


Fig. 4 — Velocity profile of $f'(\eta)$ for variation in M when $\beta = 2$.

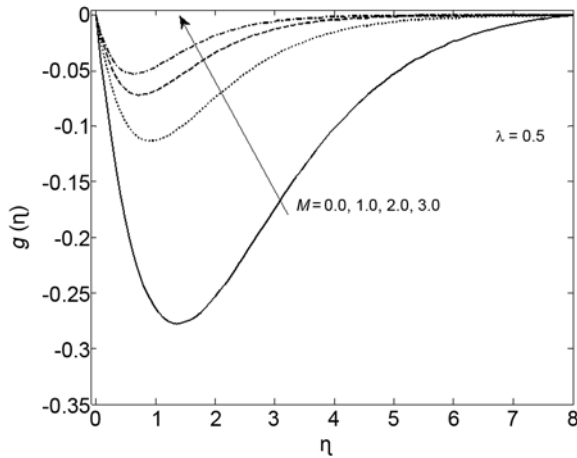


Fig. 5 — Velocity profile of $g(\eta)$ for variation in M when $\beta = 2$.

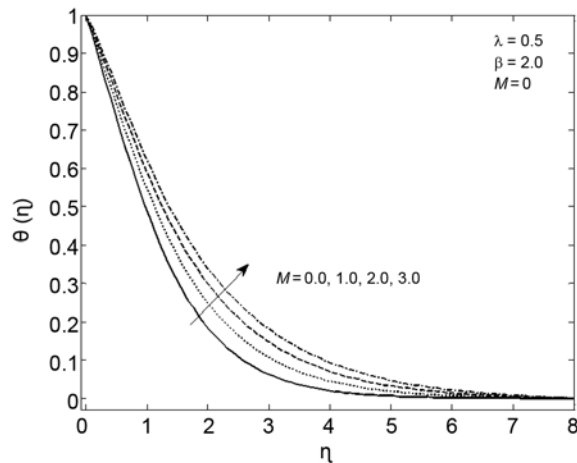


Fig. 6 — Temperature profile for variation in M when $\beta = 2$.

decreases. The results obtained in our investigation are well in agreement with Butt *et al.*³⁴ at a particular condition. In these figures for larger values of λ the

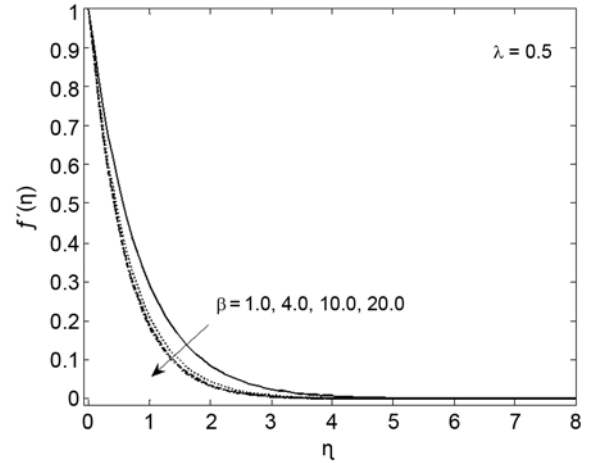


Fig. 7 — Velocity profile of $f'(\eta)$ for variation in β when $M = 2$.

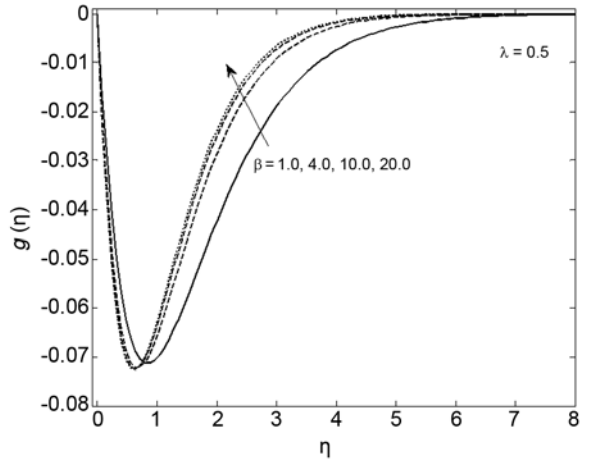


Fig. 8 — Velocity profile of $g(\eta)$ for variation in β when $M = 2$.

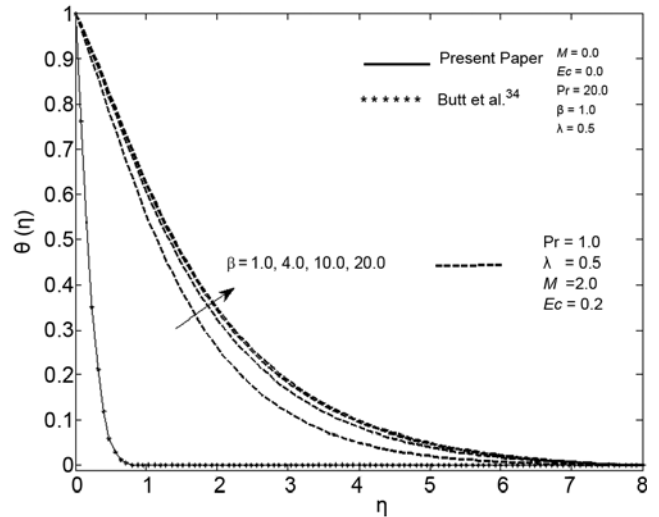


Fig. 9 — Temperature profile for variation in β when $M = 2$.

velocity profile oscillates increasingly, with no oscillation for small values of λ . On the other hand Fig. 12 illustrates that with an increase in the rotation parameter λ the temperature profile $\theta(\eta)$ increases. Hence when we increase the rotation parameter λ , the fluid temperature rises. Figure 13 exhibits the effect of Prandtl number on temperature profile $\theta(\eta)$. As value of Prandtl number Pr increases the temperature profile decreases.

Figure 14 depicts the effects of magnetic field parameter M_{ON} Ns , local entropy generation. Figure 14 shows that the local entropy generation Ns increases with increase in magnetic field parameter M . This is due to an increase in the Lorentz force. An increment in M causes enhancement of the Lorentz force and results in more friction which causes an increase in the entropy generation. Figures 15-18 show variation of rotation

parameter λ and group parameter $Br\Omega^{-1}$ on Ns and Be . It is observed that increment in both the parameters, increases the entropy generation number whereas the Bejan number decreases.

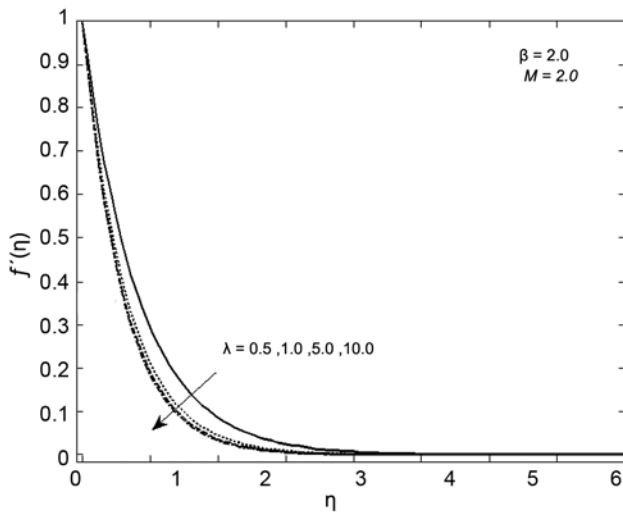


Fig. 10 — Velocity profile of $f'(\eta)$ for variation in λ when $\beta = 2$.

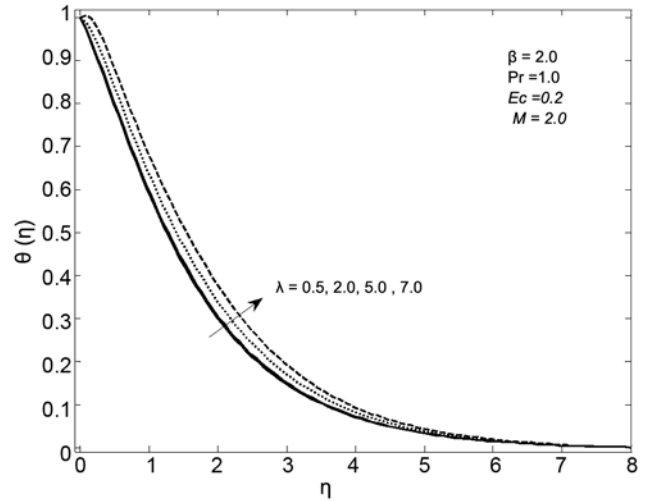


Fig. 12 — Temperature profile for variation in λ when $\beta = 2$.

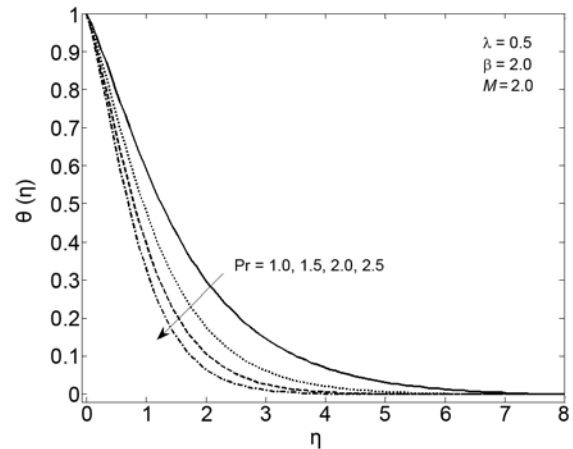


Fig. 13 — Temperature profile for variation in Pr when $\beta = 2$.

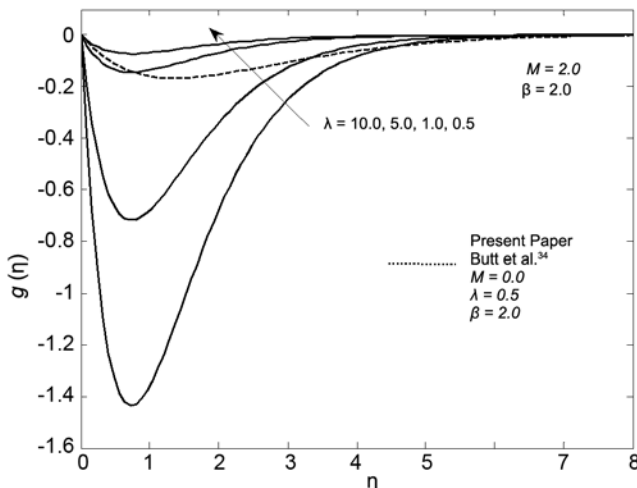


Fig. 11 — Velocity profile of $g(\eta)$ for variation in λ when $\beta = 2$.

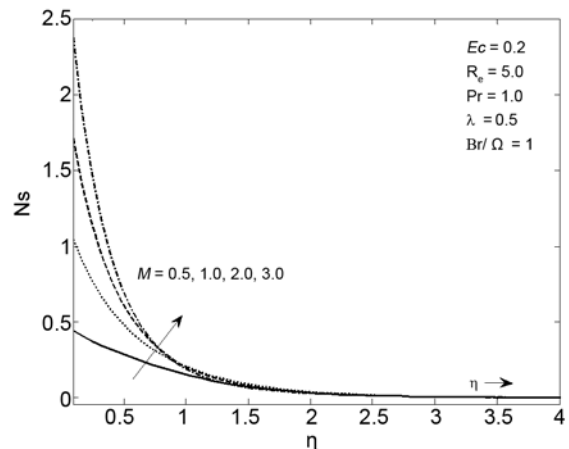


Fig. 14 — Entropy effects of Ns for variation in M when $\beta = 2$.

It is observed that the magnetic field effect and fluid friction are prominent near the stretching surface. In the region away from stretching surface, entropy due to heat surface is prominent.

Table 4 shows variation of magnetic field parameter M , rotation parameter λ and Casson fluid parameter β on

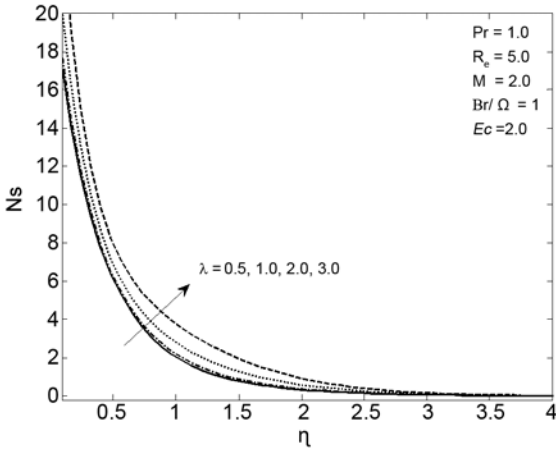


Fig. 15 — Entropy effects of N_s for variation in λ when $\beta = 2$.

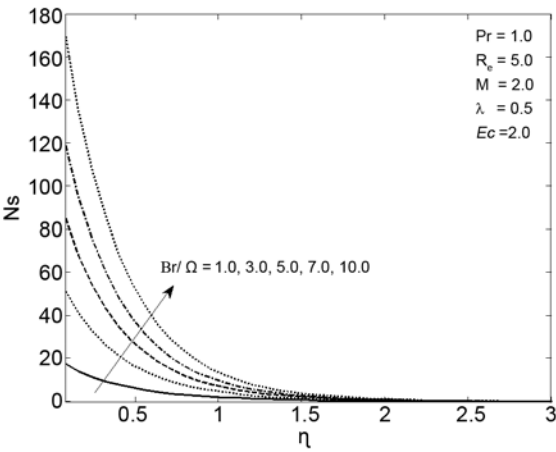


Fig. 16 — Entropy effects of N_s for variation in $Br\Omega^{-1}$.

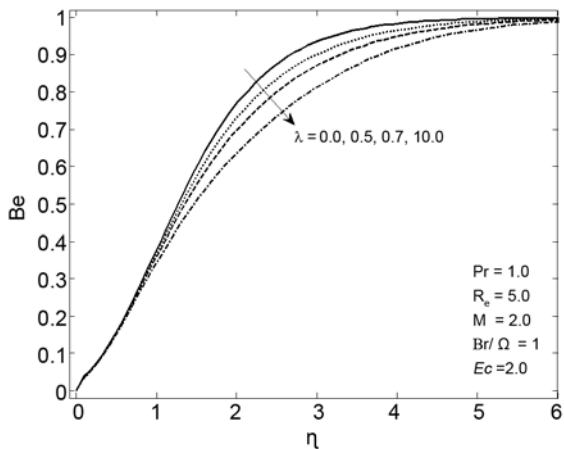


Fig. 17 — Entropy effects of Be for variation in λ when $\beta = 2$.

the skin friction coefficient $Re_x^{1/2}C_{fx}$ along the x direction and $Re_x^{1/2}C_{fy}$ along the y direction. From Table 4 it is noted that with an increase in magnetic field parameter M , the coefficient of skin friction along the x direction decreases whereas along the y direction it increases. However with an increment in the Casson fluid parameter β the skin friction coefficient increases. For an increment in the rotation parameter λ , $Re_x^{1/2}C_{fx}$ decreases. Table 5 shows variation of Nusselt number for different values of parameters. Nusselt number increases for increasing values of Prandtl number Pr but decreases as we increase the Casson fluid parameter β , Eckert number Ec , magnetic field parameter M and rotation parameter λ .

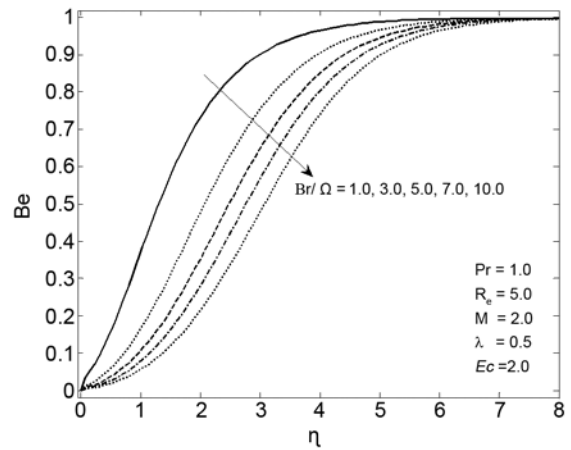


Fig. 18 — Entropy effects of Be for variation in $Br\Omega^{-1}$.

Table 4 — Numerical values of $Re_x^{1/2}C_{fx}$ and $Re_x^{1/2}C_{fy}$ for different values of rotation parameter λ , magnetic field parameter M and Casson fluid parameter β .

M	β	λ	$Re_x^{1/2}C_{fx}$	$Re_x^{1/2}C_{fy}$
0.0	2.0	0.5	-1.39647	-0.63483
1.0	2.0	0.5	-1.73205	-0.48028
2.0	2.0	0.5	-2.12132	-0.37947
3.0	2.0	0.5	-2.44648	-0.32394
2.0	2.0	0.5	-2.12132	-0.37947
2.0	4.0	0.5	-1.93649	-0.34673
2.0	10	0.5	-1.81659	-0.32550
2.0	20	0.5	-1.77482	-0.31810
2.0	2.0	0.5	-2.12132	-0.37947
2.0	2.0	1.0	-2.43251	-0.75894
2.0	2.0	5.0	-4.01253	-3.79475
2.0	2.0	10.0	-9.65421	-7.58948

Table 5 — Numerical values of $Re_x^{-1/2} Nu_x$ for different values of rotation parameter λ , magnetic field parameter M , Casson fluid parameter β , Eckert number Ec and Prandtl number Pr .

Ec	M	Pr	β	λ	$Re_x^{-1/2} Nu_x$
0.0	0.0	25	2.0	0.5	3.70075
0.2	0.0	25	2.0	0.5	2.57065
0.4	0.0	25	2.0	0.5	1.44055
0.2	0.0	25	2.0	0.5	2.57065
0.2	1.0	25	2.0	0.5	2.08139
0.2	2.0	25	2.0	0.5	1.55142
0.2	3.0	25	2.0	0.5	1.06187
0.2	2.0	25	2.0	0.5	1.55142
0.2	2.0	30	2.0	0.5	1.60113
0.2	2.0	40	2.0	0.5	1.65538
0.2	2.0	50	2.0	0.5	1.67059
0.2	2.0	25	2.0	0.5	1.55142
0.2	2.0	25	4.0	0.5	1.23850
0.2	2.0	25	10.0	0.5	0.99523
0.2	2.0	25	20.0	0.5	0.90160
0.2	2.0	25	2.0	0.5	1.55142
0.2	2.0	25	2.0	1.0	1.43173
0.2	2.0	25	2.0	2.0	0.95297
0.2	2.0	25	2.0	3.0	0.15505

6 Conclusions

The current study focused on investigation of entropy generation for three dimensional MHD boundary layer flow and heat transfer due to a stretching surface in a rotating Casson fluid. Some important results are as follows:

The parallel velocity profiles $f'(\eta)$ and $g(\eta)$ in the x and y directions decrease as the Casson fluid parameter β and magnetic parameter M increase.

The velocity profiles $f'(\eta)$ and $g(\eta)$ decrease as the rotation parameter λ increases.

An increment in the Casson fluid parameter β , magnetic field parameter M and rotation parameter λ increases the thermal boundary layer thickness. On the other hand an increment in Prandtl number Pr , decreases the noted in temperature profile.

The local entropy generation number N_s increases with increase in magnetic field parameter M , rotation parameter λ and group parameter $Br\Omega^{-1}$. On the other hand Bejan number Be decreases as the rotation parameter λ and group parameter $Br\Omega^{-1}$ increase.

For an increase in magnetic field parameter M , the coefficient of skin friction along the x direction decreases whereas along they direction it increases.

The skin friction coefficients $Re_x^{1/2} C_{fx}$ and $Re_x^{1/2} C_{fy}$ in the x and y directions increase with the Casson fluid

parameter β whereas $Re_x^{1/2} C_{fx}$ decreases and $Re_x^{1/2} C_{fy}$ increases with magnetic field parameter M .

Net heat transfer through the flow decreases with the increasing value of M .

Acknowledgement

The support provided by Manipal University Jaipur through Endowment Fund Fellowship to one of the author RC is gratefully acknowledged.

References

- Crane L J, *Zeit Ange Math und Phys*, 21 (1970) 645.
- Sakiadis B C, *AIChE J*, 7 (1961) 26.
- Wang C Y, *Phys Fluids*, 27 (1984) 1915.
- Verma P D & Chauhan D S, *Indian J Pure Appl Math*, 10 (1979) 1351.
- Jain S, *J Rajasthan Acad Phys Sci*, 5 (2006) 477.
- Fang T, Zhang J & Yao S, *Commun Nonlinear Sci Numer Simul*, 14 (2009) 3731.
- Najar R, Amin N & Pop I, *Mech Res Commun*, 31 (2004) 121.
- Mahanta G & Shaw S, *Alexandria Eng J*, 54 (2015) 653.
- Jain S & Choudhary R, *Proc Eng*, 127 (2015) 1203.
- Raju C S K, Naramgari S, Babu M J & Sugunamma V, *Alexandria Eng J*, 55 (2016) 151.
- Jain S & Bohra S, *Indian J Pure Appl Phys*, 55 (2017) 847.
- Wang C Y, *Z Angew Math Phys*, 39 (1988) 177.
- Takhar H S, Chamkha A J & Nath G, *Int J Therm Sci*, 42 (2003) 23.
- Zaimi K, Ishak A & Pop I, *Appl Math Mech Engl Ed*, 34 (2013) 945.
- Mustafa M, *Int J Heat Mass Trans*, 108 (2017) 1910.
- Hayat T, Muhammad T, Shehzad S A & Alsaedi A, *Comput Meth Appl Mech Eng*, 315 (2017) 467.
- Bejan A, *CRC Press, Boca Raton*, (1996).
- Makinde O D & Osalusi E, *Entropy*, 7 (2005) 148.
- Butt A S & Ali A, *J Braz Soc Mech Sci Eng*, 37 (2015) 211.
- Freidoonimehr N, Rashidi M M, Abelman S & Lorenzini G, *Entropy*, 18 (2016) 131.
- Qing J, Bhatti M M, Abbas M A, Rashidi M M & Ali M El-S, *Entropy*, 18 (2016) 123.
- Casson N A, *Rheology of disperse systems*, (Pergamon Press: Oxford), 1959.
- Boyd J, Buick J M & Green S, *Phys Fluids*, 19 (2007) 93.
- Bhargava R, Takhar H S, Rawat S, Beg T A & Beg O A, *Nonlinear Anal Model*, 12 (2007) 317.
- Attia H A & Ahmed M E S, *Italian J Pure Appl Math*, 27 (2010) 19.
- Mukhopadhyay S, *Chin Phys B*, 27 (2013) 074701.
- Nadeem S, Haq R U & Lee C, *Scientia Iranica B*, 19 (2012) 1550.
- Bhattacharyya K, T Hayat & Alsaedi A, *Chin Phys B*, 22 (2013) 024702.
- Mukhopadhyay S, Mondal I C & Chamkha A J, *Heat Trans Asian Res*, 42 (2013) 665.
- Nadeem S, Haq R U, Akbar N S & Khan Z H, *Alexandria Eng J*, 52 (2013) 577.

- 31 Pramanik S, *Ain Shams Eng J*, 5 (2014) 205.
- 32 Tufail M N, Butt A S & Ali A, *Indian J Phys*, 1 (2014) 75.
- 33 Sumalatha C & Bandari S, *World J Mech*, 5 (2015) 257.
- 34 Butt A S, Ali A & Mehmood A, *Proc Natl Acad Sci India*, 85 (2015) 421.
- 35 Jain S & Bohra S, *Adv Math Phys*, 2016 (2016) 9671513.
- 36 Ali F, Sheikh N A, Khan I & Saqib M, *J Magn Magn Mater*, 423 (2017) 327.
- 37 Raju C S K, Hoque M M & Sivasankar T, *Advanced Power Tech*, 28 (2017) 575.